doi: 10.1038/nature07159

Supplementary Figures with Legends

Molecular architecture of native HIV-1 gp120 trimers

Jun Liu*, Alberto Bartesaghi*, Mario Borgnia*, Guillermo Sapiro[f] and Sriram Subramaniam

Laboratory of Cell Biology,
Center for Cancer Research,
National Cancer Institute, NIH
Bethesda, MD 20892.

and

[f]Department of Electrical and Computer Engineering
University of Minnesota, Minneapolis, MN

* These authors contributed equally to this work

Address for correspondence: Sriram Subramaniam (ss1@nih.gov)

Supplementary figure legends

Fig. S1: Cryo-electron tomography of HIV-1. (a,b) Slice through a representative tomogram obtained from plunge-frozen virions of HIV-1 strain BaL. Scale bar is 100 nm wide. (b) Segmented rendering of a single HIV-1 virion showing the viral membrane (blue), core (yellow) and surface spikes (red). The trimeric architecture of the surface spike is clearly visible in some of the spikes. (c) Fourier shell correlation plots for the final maps of the trimeric spike on HIV-1 in the free state, in complex with the Fab fragment of b12, and in complex with CD4 and the Fab fragment of 17b. The resolution at which the Fourier shell correlation drops to 0.5 (~ 19 Å, 22 Å and 23 Å, for maps in Figs. 1, 2 and 3 respectively) is taken to represent the resolution limit of the density maps.

Fig. S2: An example of the classification of spike volumes extracted from data collected using viruses complexed to the b12 Fab fragment. An early stage of the classification (third round of iteration) is shown to illustrate that the classification scheme used here results in clear separation of spikes with and without bound fragments. The set of ~ 4300 spikes is divided into 10 classes in the example shown, before (a) and after (b) application of 3-fold symmetry. The top 5 classes which were used to construct the references for the next round of alignment and classification show the presence of the additional density feature (the spokes on the periphery of the spike) from the bound Fab fragment more clearly than the bottom 5 classes. Each row corresponds to a single 3D class average, and includes a small number of sections at the levels where the gp120 density is most prominent. The first two columns show lateral projection views separated by 90 degrees, and the remaining columns correspond to 4.1 Å thick slices oriented perpendicular to

the spike axis. The classes, as well as the final map indicate a stoichiometry of 3 b12 Fab fragments for 3 gp120 molecules. Since the final average is derived from thousands of individual spike density maps, each at a very low signal-to-noise ratio, it is difficult to precisely determine whether every spike contributing to the map is at full stoichiometry, especially since the classification procedures we used select for those at or near maximal occupancy.

Fig. S3: Improvement in quality of the map of the gp120-b12 complex shown in Fig. 1 with successive steps in refinement. The first row shows the starting global average (iteration 0) and each of the subsequent rows show the averaged map after each of the 14 refinement iterations. The first column shows a vertical cross-section along the central axis of the spike and columns to the right show consecutive sections orthogonal to the vertical axis of the spike across a region that spans the b12 binding site.

Fig. S4: Quantitation of coordinate fits to density maps of complexed and unliganded spikes derived by cryo-electron tomography combined with 3D averaging. The plots show the landscape of correlation coefficients for fits between the coordinates and the experimentally derived density map as a function of orientation. The landscapes are shown as 3D surfaces along which correlation coefficients are constant, with levels selected to show both the general shape (blue) and the location of the peak (red) that corresponds to the global maximum for each of the fits. The axes represent the three Euler angles needed to capture the entire rotational space in 3D sampled on a uniform grid with 3-degree increments. Each point in the grid represents a distinct rotation in 3D of the X-ray coordinates. Correlation coefficients were computed between the X-ray

coordinates at each of these orientations and the density map, ensuring that the spatial displacement for each orientation was optimized. This effectively corresponds to an exhaustive six-dimensional search of the global maximum in fit between the coordinates and the map. The peaks in panels (a), (b) and (c) correspond to values of 0.81, 0.73 and 0.76 respectively, for the correlation coefficients; values of the blue threshold shown are 0.66, 0.63 and 0.57, respectively. (a) Peak corresponding to fit of the gp120-b12 complex into the density map presented in Fig. 1. (b) Peak corresponding to fit of HIV-1 gp120 coordinates 1GC1 into the density map presented in Fig. 2. Residues in loop regions were not considered to determine the fit. (c) Peak corresponding to fit of the gp120/CD4/17b complex into the density map presented in Fig. 3.

Fig. S5: Fit of gp120 coordinates to density map of HIV-1 BaL spike, displayed at the same threshold as that used in Figs 2d-f. Density maps corresponding to the structures available for the truncated gp120 core were computed at 20 Å resolution (a-c) and these were fit into the experimentally determined density maps for the native spike using automated fitting functions implemented in the software package Chimera; front (d-f) and top (g-i) views are shown. The map orientation is identical in panels (a) – (f), and orthogonal to the orientation shown in panels (g) - (i). Visual inspection shows that the shapes of the 2NY7 and 1GC1 coordinates follow the shape of the experimentally determined map, while the 2BF1 coordinates do not show obvious shape complementarity. The yellow spheres indicate the likely positions of the V1/V2 loop regions based on location of the corresponding truncated stumps in the coordinates. In the 2NY7 and 1GC1 coordinates, the estimated location of the V1/V2 loop region shows an excellent correspondence to the region of unassigned density at the apex of the spike, while the estimated

location of this loop region in the 2BF1 coordinates falls in a region where there is no unassigned density, and is not consistent with the observed architecture of the spike. All three sets of coordinates have significant deletions in the N and C-terminal regions which are expected to reside at the base of the spike, corresponding to the unassigned density visible in the map. The qualitative result that the 2NY7 and 1GC1 coordinates provide a good model for the structure of the monomer in the unliganded spike is further confirmed by calculation of the number of atoms that are included in the map over a range of density thresholds. For this purpose, the three sets of coordinates were fitted to the map as shown in the map panels, and the contour values at which the map and coordinates were visualized were progressively varied. At each contour value, the proportion of atoms that fell outside the map contour was calculated using Chimera. The plot shows that compared to the fits obtained using 2NY7 or 1GC1 coordinates, a substantially higher proportion of atoms are distributed outside the map contour when 2BF1 coordinates are used to carry out the fit in the orientation roughly corresponding to that suggested by Chen et al (*Nature* 433, 834-841 (2005)).

Fig. S6: Comparison of the fits of 2NY7, 1GC1 and 2BF1 coordinates to the density map of the unliganded HIV-1 spike at a series of threshold levels to further highlight why the coordinates reported by Chen et al (*Nature* 433, 834-841 (2005)) for the truncated SIV monomeric core (2BF1) do not match the density of gp120 in the native trimer, while the coordinates for the liganded truncated HIV-1 gp120 core (2NY7 or 1GC1) fit over the entire range of thresholds. The yellow spheres indicate the locations of the V1/V2 loop regions in the different fits. This figure is a structural version of the plot shown in Fig. S5. The fits are to the density map and not the thresholded surface, and are therefore

identical across all thresholds. In contrast to the HIV-1 gp120 coordinates, the use of SIV gp120 (2BF1) coordinates produces fits with significantly lower correlation coefficients, and a landscape without a clear maximum. The top five peaks (CCC ranging from 0.695 to 0.685) correspond to trimer architectures that are unlikely to be physiologically meaningful because they either have the N- and C-termini of gp120 located near the apex or the upper half of the spike, or have the V1/V2 loop regions or the bulk of the glycoslated surface of gp120 buried in the interior of the spike close to the membrane. The local maximum near the orientation corresponding to the conformation of the trimer proposed by Chen et al (and replicated in panels in the third column of Figs. S5 and S6) has a correlation coefficient of 0.68, and cannot account for the presence of the large densities at the apex of the spike.

Fig. S7. Comparison of density map reported here for spikes seen on HIV-1 BaL with those previously reported by Zhu et al (*Nature* **441**, 847-852 (2006)) and by Zanetti et al (*PLoS Pathog* **2**, e83 (2006)) for spikes seen on tail-truncated SIVmac239 viruses (permission to reproduce these figures will be obtained). The splayed legs in the membrane proximal region of gp41 that are separated from each other by ~ 80Å, as reported by Zhu et al are not confirmed in our work. The map we present in Fig. 2 bears a resemblance to the map reported by Zanetti et al, in the stalk region, although this map has the opposite handedness to our maps. Note the handedness of the maps we present in Figs 1-3 is uniquely determined because of the constraints provided by the bound b12 and CD4/17b proteins. In addition to the differences in global spike architecture, we note that these two earlier reports interpreted the maps in terms of the structure reported for

the unliganded SIV gp120 monomer (Chen et al *Nature* 433, 834-841 (2005)), which does not fit the density maps reported in the present study, as illustrated in Figs. S5 and S6.

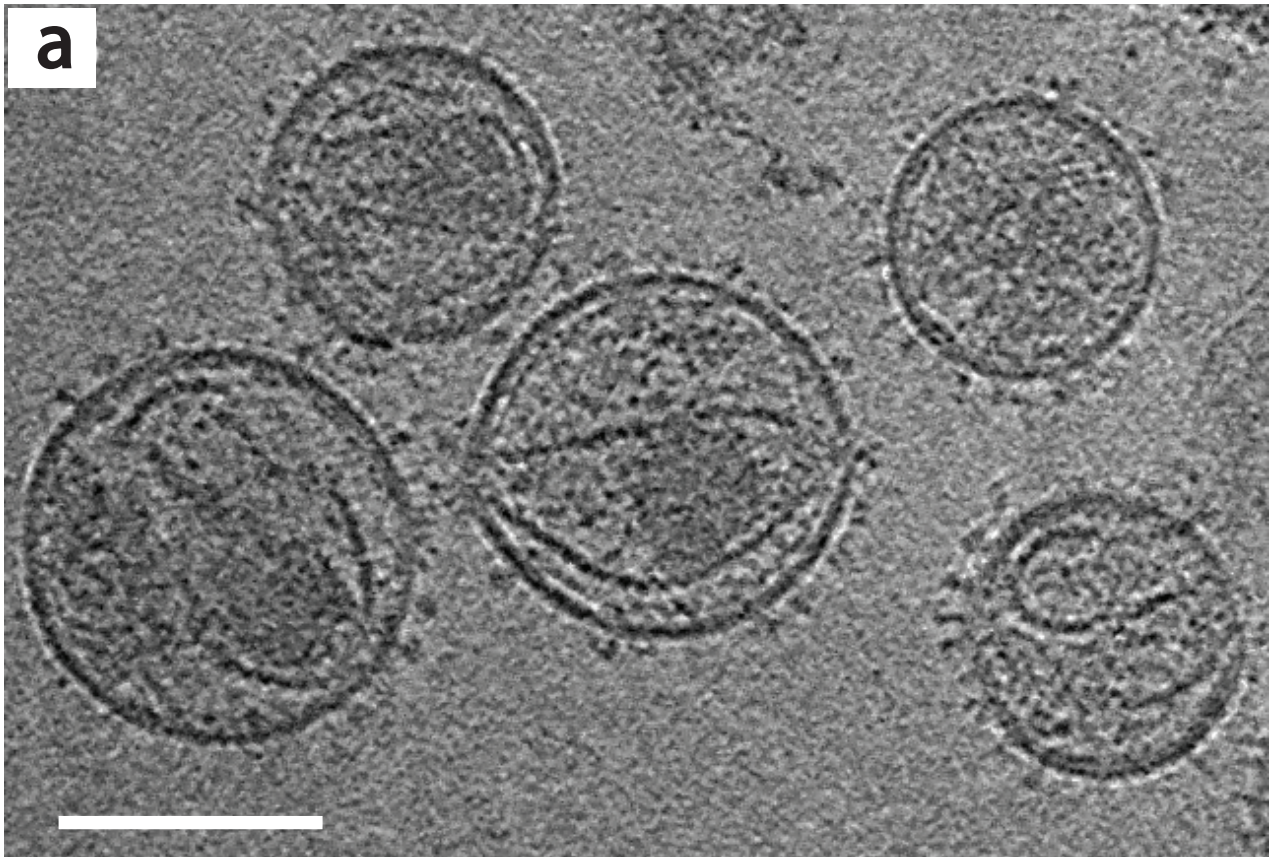
a

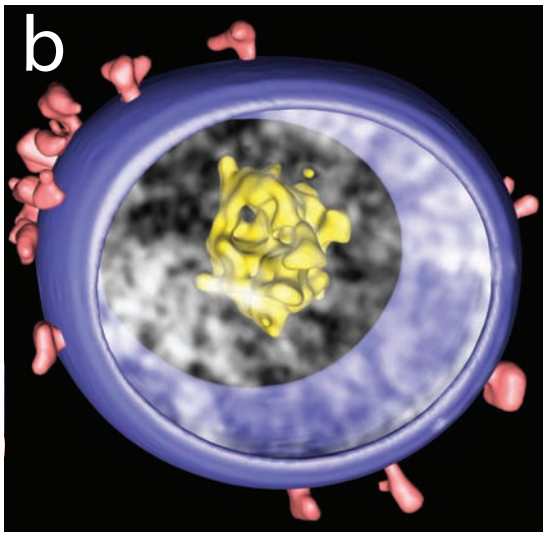
b

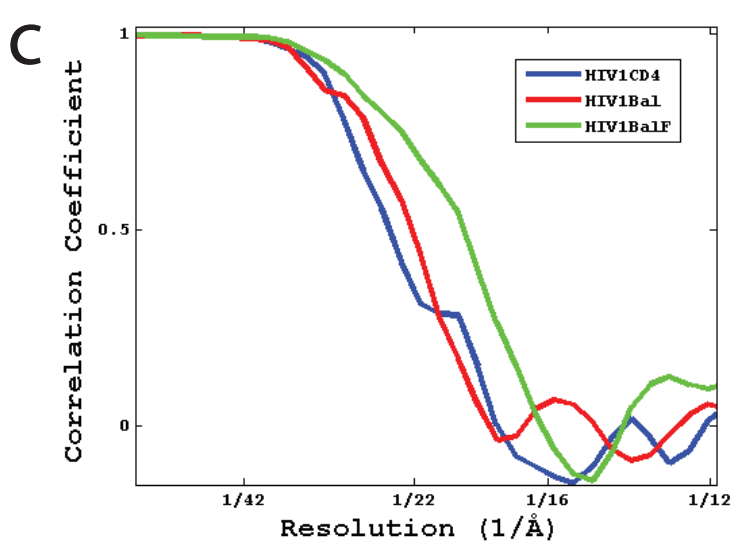
c
Correlation Coefficient
1
0.5
0
HIV1CD4
HIV1Bal
HIV1BalF
1/42
1/22
1/16
1/12
Resolution (1/Å)

Figure S1

a

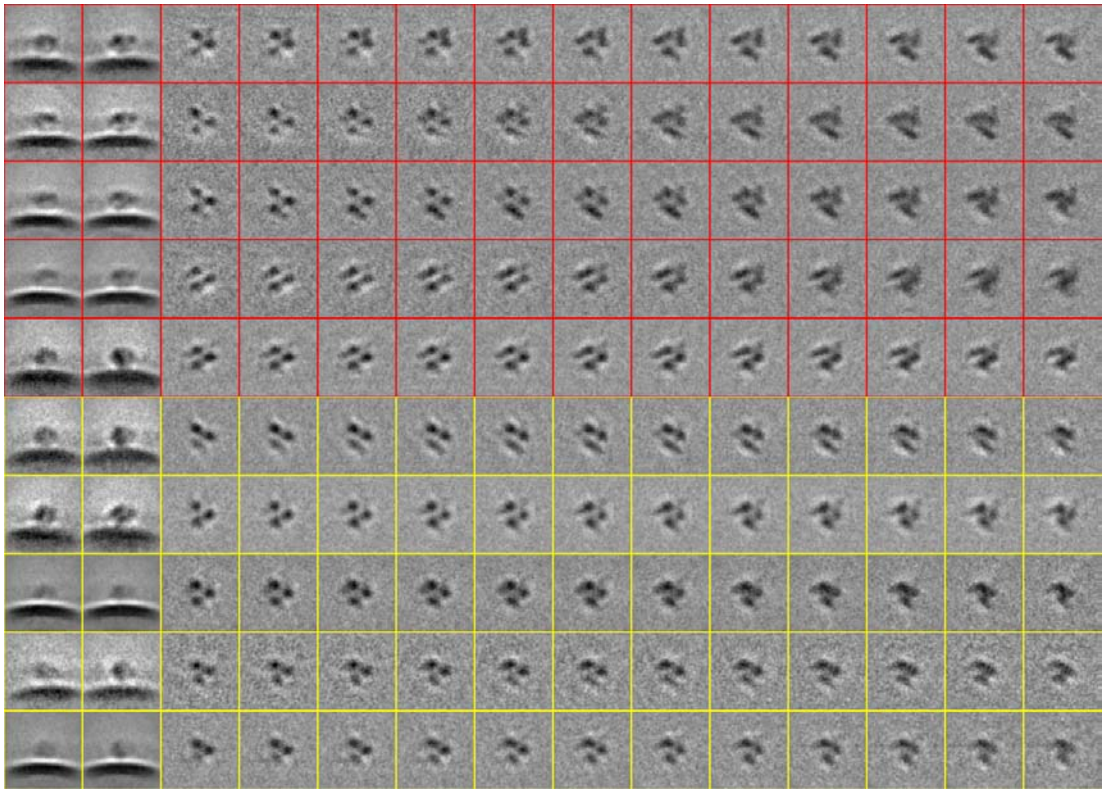

b

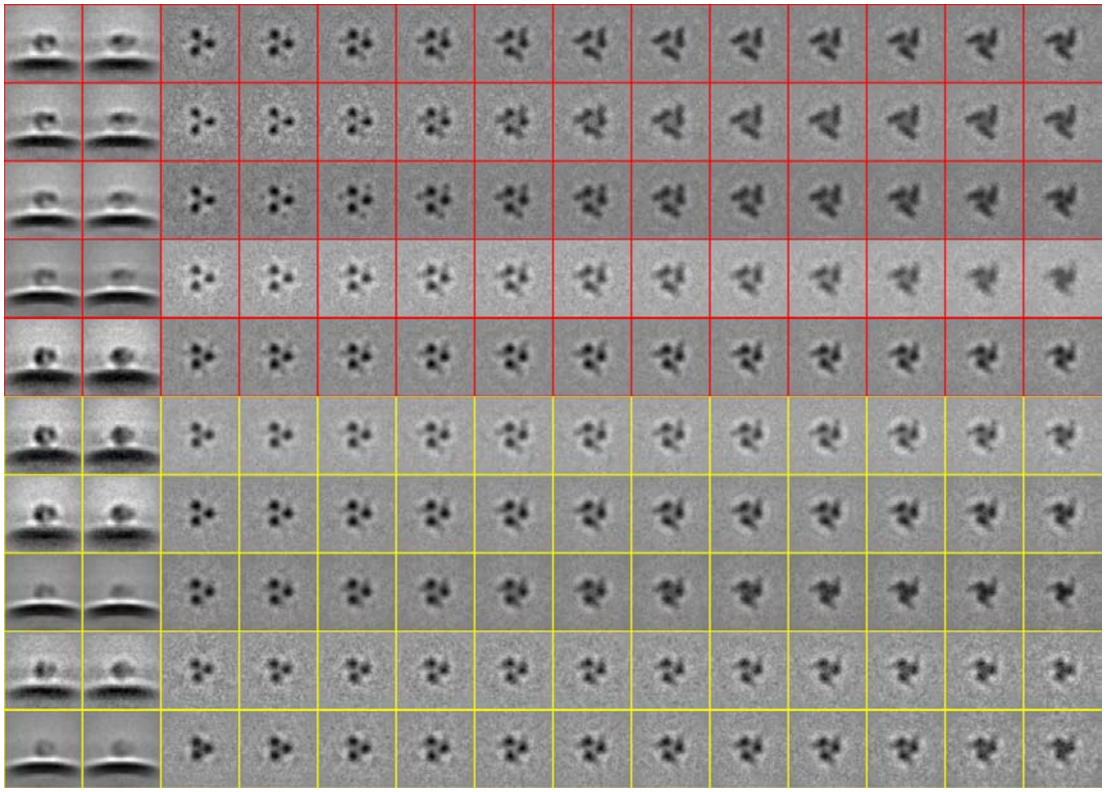

Figure S2

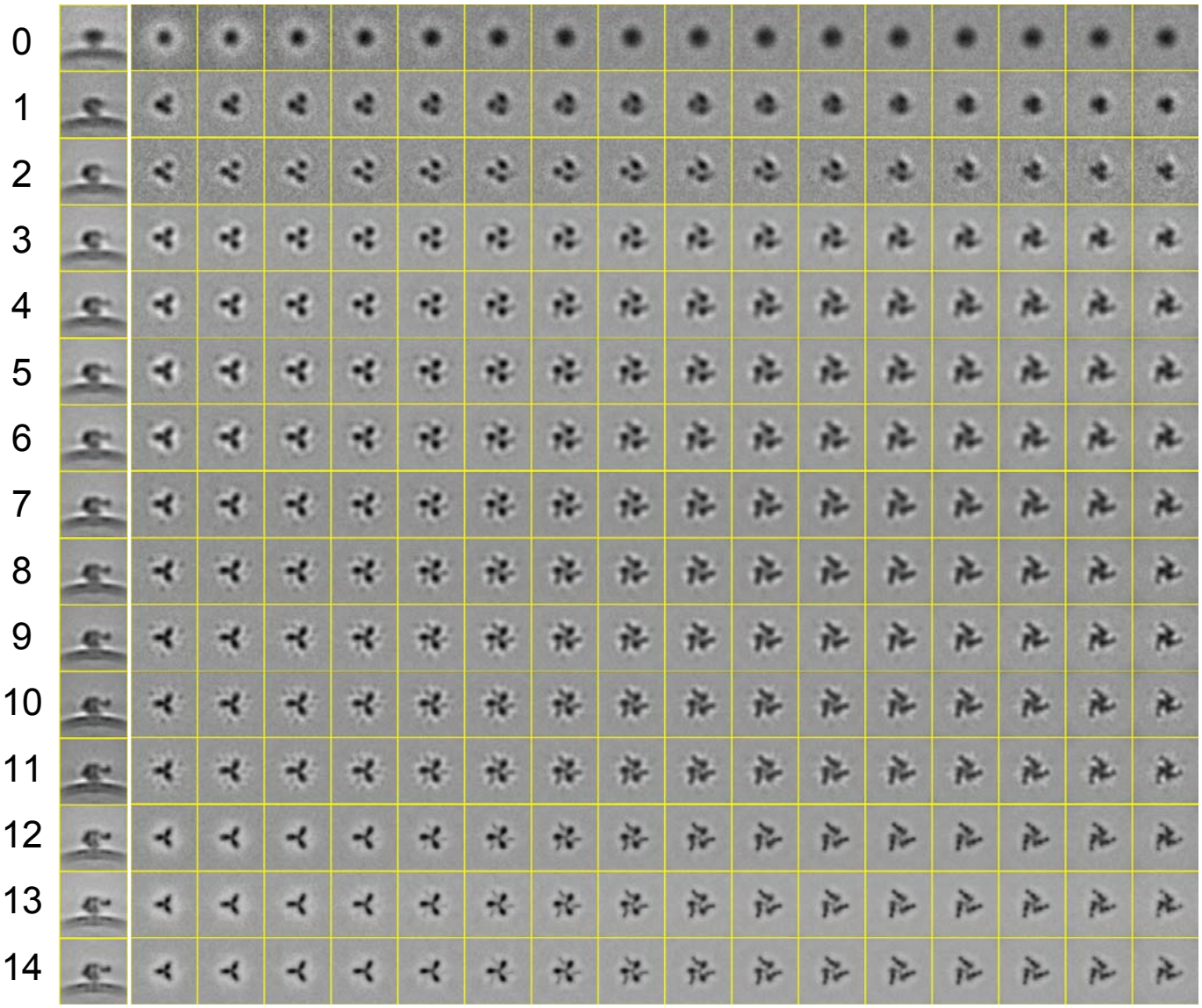

Figure S3

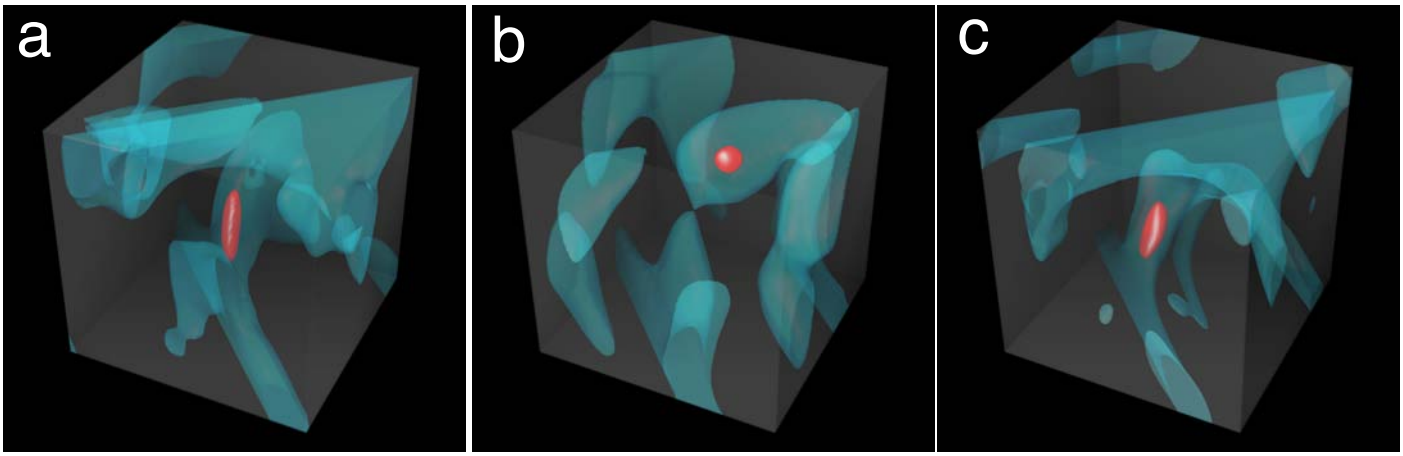

Figure S4

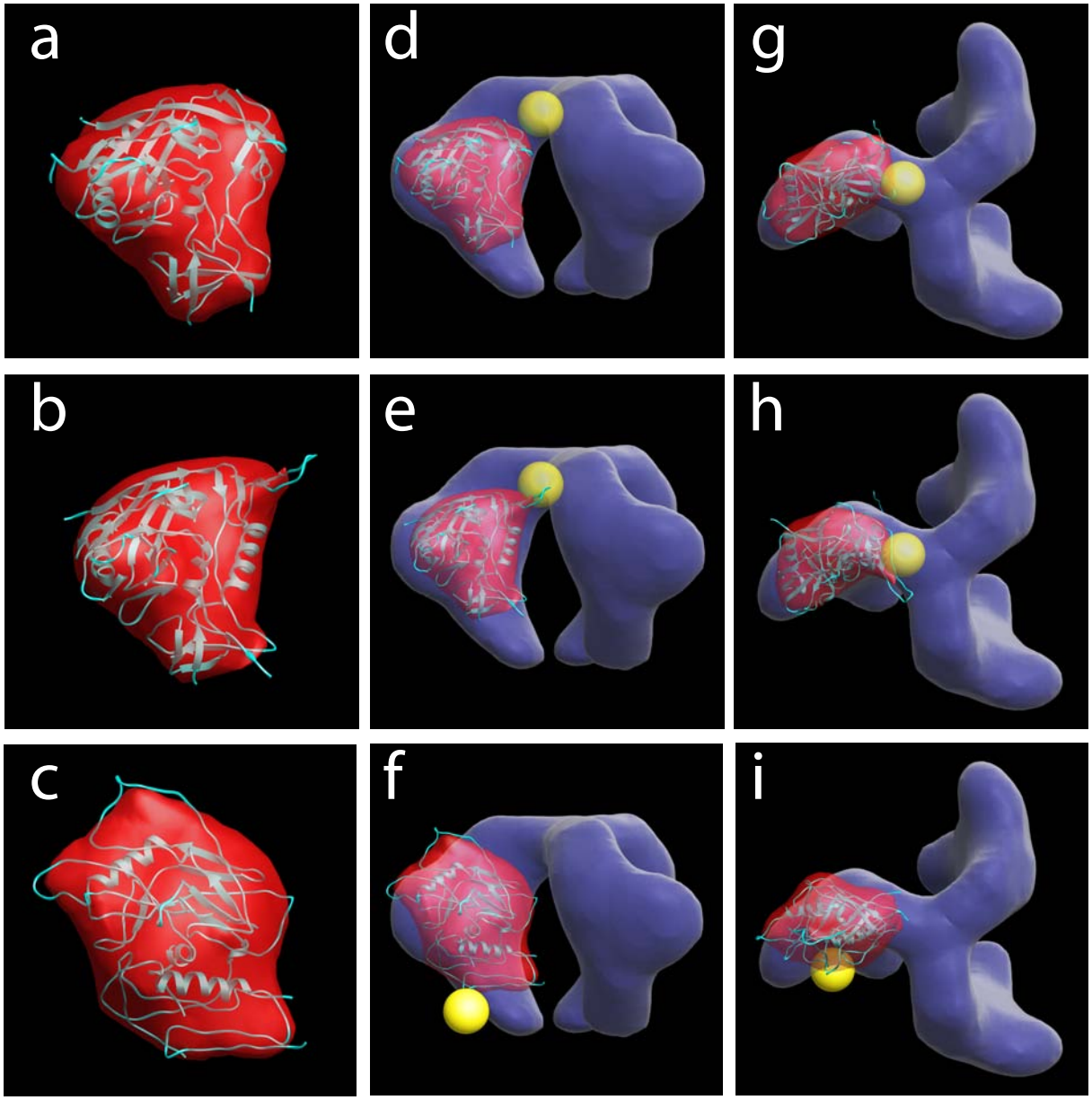
a
d
g
b
e
h
c
f
i

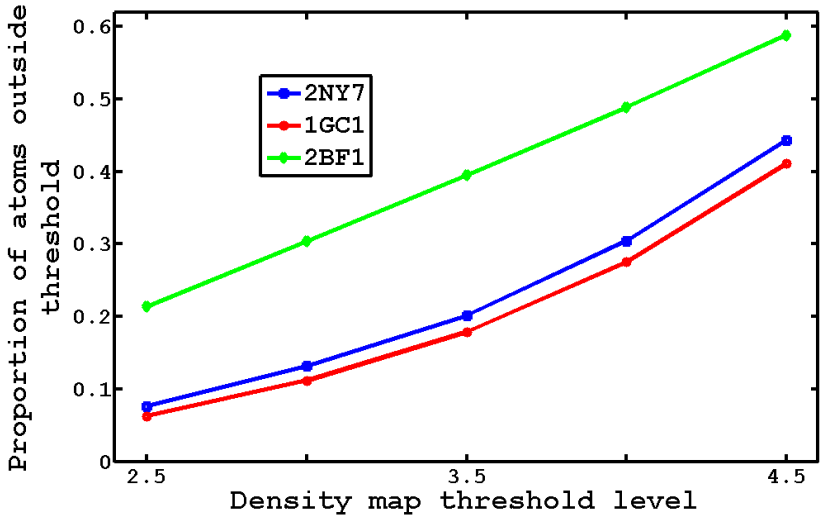
Proportion of atoms outside threshold
0.6
0.5
0.4
0.3
0.2
0.1
0
2NY7
1GC1
2BF1
2.5
3.5
4.5
Density map threshold level

Figure S5

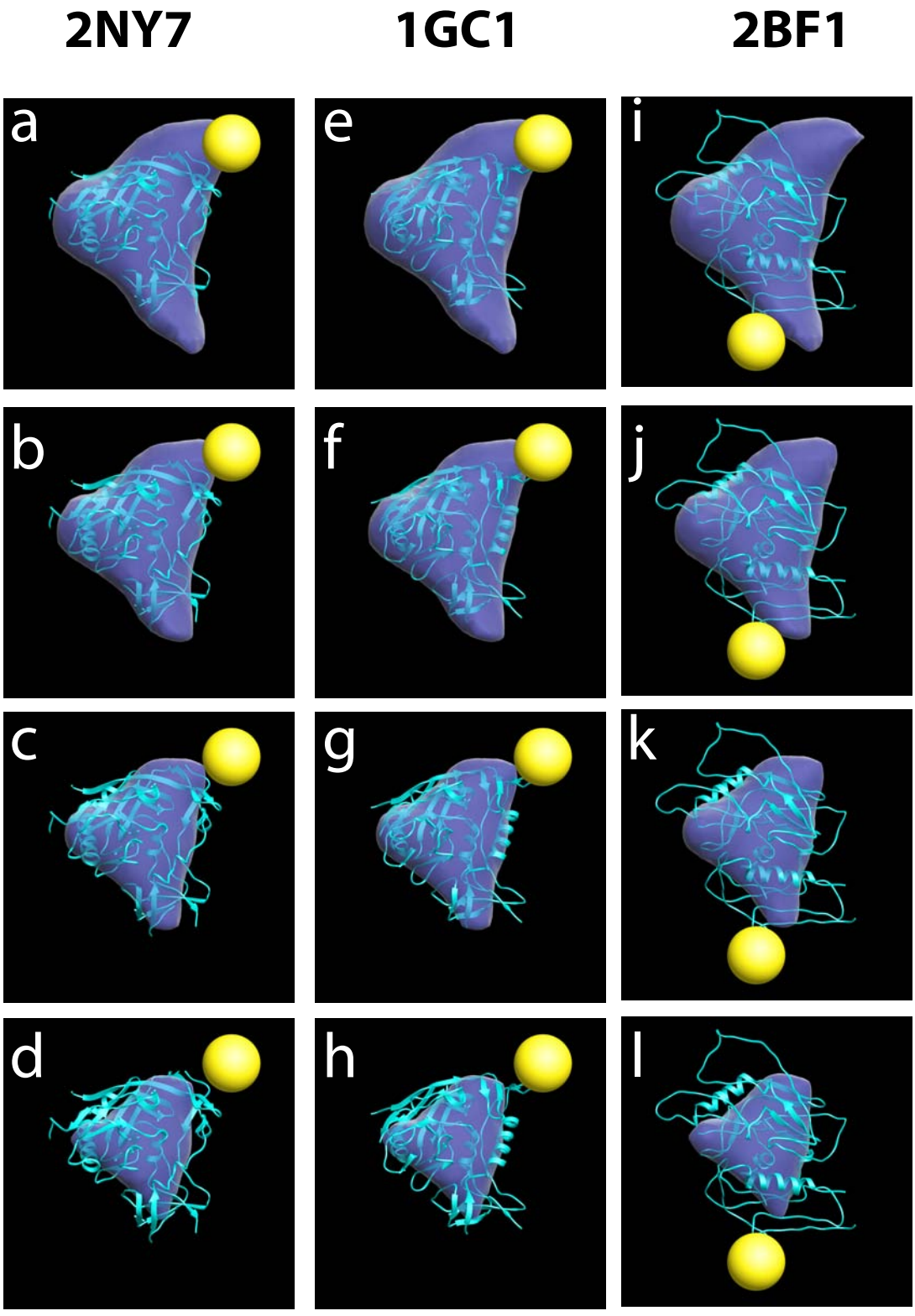

Figure S6

a

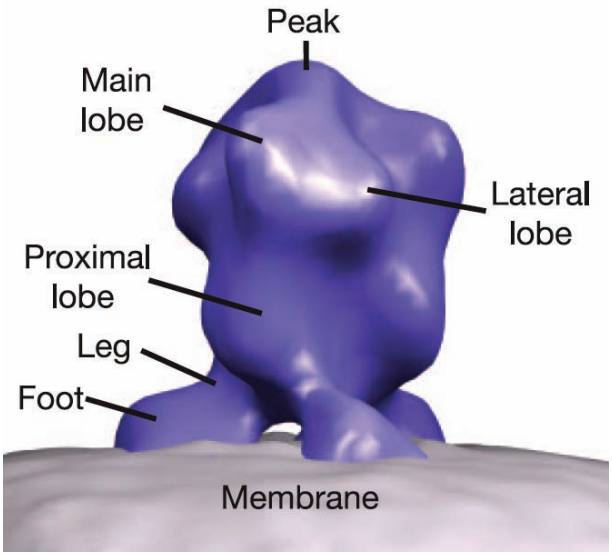

from Fig. 3 of Zhu et al.
Nature 441, 847-852 (2006)

b

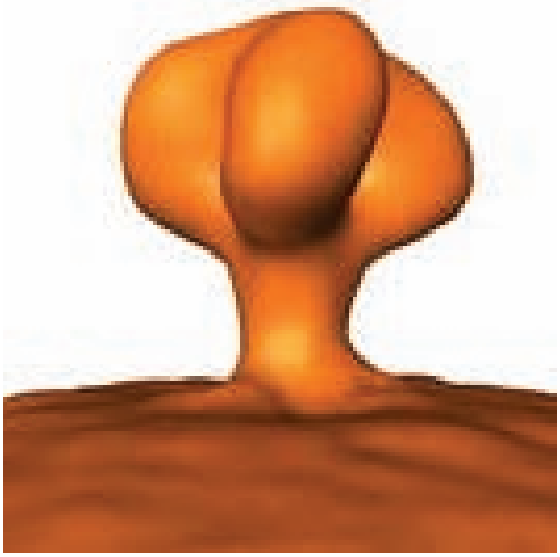

from Fig. 2 of Zanetti et al.
PLoS Pathog. 2, e83 (2006)

c

Liu et al (2008)
(present manuscript)

Figure S7